Device simulation of lead-free $CH_3NH_3SnI_3$ perovskite solar cells with high efficiency*

Hui-Jing Du(杜会静), Wei-Chao Wang(王韦超), and Jian-Zhuo Zhu(朱键卓)†

College of Science, Yanshan University, Qinhuangdao 066004, *China*

(Received 28 March 2016; revised manuscript received 21 June 2016; published online 25 August 2016)

The lead-free perovskite solar cells (PSCs) have drawn a great deal of research interest due to the Pb toxicity of the lead halide perovskite. $CH_3NH_3SnI_3$ is a viable alternative to $CH_3NH_3PbX_3$, because it has a narrower band gap of 1.3 eV and a wider visible absorption spectrum than the lead halide perovskite. The progress of fabricating tin iodide PSCs with good stability has stimulated the studies of these $CH_3NH_3SnI_3$ based cells greatly. In the paper, we study the influences of various parameters on the solar cell performance through theoretical analysis and device simulation. It is found in the simulation that the solar cell performance can be improved to some extent by adjusting the doping concentration of the perovskite absorption layer and the electron affinity of the buffer and HTM, while the reduction of the defect density of the perovskite absorption layer significantly improves the cell performance. By further optimizing the parameters of the doping concentration (1.3×10^{16} cm^{-3}) and the defect density (1×10^{15} cm^{-3}) of perovskite absorption layer, and the electron affinity of buffer (4.0 eV) and HTM (2.6 eV), we finally obtain some encouraging results of the J_{sc} of 31.59 mA/cm^2, V_{oc} of 0.92 V, *FF* of 79.99%, and *PCE* of 23.36%. The results show that the lead-free $CH_3NH_3SnI_3$ PSC is a potential environmentally friendly solar cell with high efficiency. Improving the Sn^{2+} stability and reducing the defect density of $CH_3NH_3SnI_3$ are key issues for the future research, which can be solved by improving the fabrication and encapsulation process of the cell.

Keywords: $CH_3NH_3SnI_3$, perovskite solar cells, device simulation, high efficiency

PACS: 88.40.H–, 88.40.hj, 88.40.fc **DOI:** 10.1088/1674-1056/25/10/108802

1. Introduction

In recent years, lead halide ($CH_3NH_3PbX_3$, X = Cl, Br, I) perovskite solar cells (PSCs) have drawn a great deal of attention because they have lower cost and simpler processing techniques[1–3] than traditional silicon based solar cells. In the past few years, the power conversion efficiency (PCE) of $CH_3NH_3PbX_3$ PSC has been significantly enhanced from 3.8% in 2009[4] to 221% in 2016.[5] Despite the significant progress of the PSCs, the toxicity of lead remains a major obstacle to the wide application of these PSCs. Experimental and theoretical studies show that $CH_3NH_3SnI_3$ has a narrower band gap of 1.3 eV,[6,7] which can cover a wider range of the visible spectrum, than the band gap of the lead halide perovskite (1.55 eV). First-principles study indicates that $CH_3NH_3SnI_3$ is a promising perovskite absorber in the highly efficient solar batteries with the best optical properties and the widest light-adsorption range in all the $CH_3NH_3BX_3$ (B = Sn, Pb; X = Cl, Br, I) compounds.[8] As a lead-free alternative, tin-based perovskites have been applied to solar cells with planar heterojunction architecture.[9–14] However, these devices degrade rapidly in the air. This is mainly attributed to the easy oxidization of Sn^{2+} into Sn^{4+}, which greatly restricts the development of the tin-based PSCs. Recently, with the development of the fabrication and encapsulation process, the stability of the $CH_3NH_3SnI_3$ based cells has been improved. The addition of SnF_2 in the system reduces the Sn^{4+} caused by the oxidation of Sn^{2+}.[14] $FASnI_3$ PSC with high duplicability has been fabricated with SnF_2 as an inhibitor of Sn^{4+}, and the encapsulated device has exhibited a stable performance for over 100 days, maintaining 98% of its initial efficiency.[9] This strategy is now commonly applicable to the fabrication of Sn-based PSC. Moreover, by chemical substitution of I by Br in the form of the solid solution $CH_3NH_3SnI_{3-x}Br_x$, the band gap can be tuned to cover a wide range of the visible spectrum. Thus, the Sn-based hybrid perovskites could be a promising alternative to the Pb-based light-harvesting materials,[14,15] and this provides an opportunity to develop lead-free solar cells with high efficiency.

In spite of the progress of the stability improvement in the Sn-based PSCs, the *PCE* of the $CH_3NH_3SnI_3$ based PSCs is still very low, so it is necessary to understand the relationship between the structure parameters and the cell performance deeply. Yet to date, there has been no report on the device simulation of $CH_3NH_3SnI_3$ based PSCs. Simulation methods allow intuitive examination of each parameter in solar cells and thus identify the optimal conditions for operating.[16–20] In this paper, the factors affecting the lead-free $CH_3NH_3SnI_3$ PSC efficiency are analyzed by one-dimensional device simulation with SCAPS (ver.3.3.02) under AM1.5G illumination. The solar cell capacitance simulator (SCAPS) is a general so-

*Project supported by the Graduate Student Education Teaching Reform Project, China (Grant No. JG201512) and the Young Teachers Research Project of Yanshan University, China (Grant No. 13LGB028).

†Corresponding author. E-mail: zhujz@ysu.edu.cn

© 2016 Chinese Physical Society and IOP Publishing Ltd

lar cell simulation program that is based on three basic semiconductor equations and it is well adapted to modeling various hetero- and homo-junctions, multi-junction, and Schottky barrier devices.[18–20]

2. Device simulation parameters

In the $CH_3NH_3SnI_3$ based solar cell adopted is a planar heterojunction architecture with layer configuration of glass substrate/TCO/buffer layer TiO_2(ETM)/absorption layer $CH_3NH_3SnI_3$/hole transport material (HTM) spiro-OMeTAD /metal back contact (see Fig. 1). Note that the main material parameters are carefully selected from those reported in experimental data and other theoretical results.[7–10,17–21] Table 1 summarizes the primary parameters for each layer in the simulation. The unmarked parameters of TCO, buffer and HTM layers are cited from the simulation literature about PSCs.[7,17–21] Thermal velocities of the electron and hole are both set to be equal to 10^7 cm/s. The defects in the absorption layer are set to be in the neutral Gaussian distribution with a characteristic energy of 0.1 eV, and the defect energy level is at the center of the band gap. To consider the interface carrier recombination, we insert defect interfaces into the buffer/absorber and the absorber/HTM respectively. The interface defects are set to be single and neutral defect with a total density of 1×10^{17} cm^{-3}, located at 0.6 eV above the top of valence band E_v. The parameter setting of the defects in the simulation is shown in Table 2. Pre-factor A_α is 10^5 to obtain the absorption coefficient (α) curve calculated by $\alpha = A_\alpha(h\nu E_g)^{1/2}$. The optical reflectance neither at the surface nor at the interface of each layer is considered in this simulation.

Our study focuses on the effects of the doping concentration, the defect density and the thickness of the perovskite absorber layer, and the electron affinity χ of the ETM and the HTM. The control variable method is used in the study during the parameter optimization. The initial parameters are shown in Table 1. The initial defect density N_t of the absorber is set to be 4.5×10^{17} cm^{-3}, because on this condition the simulated carrier diffusion length of 30 nm is similar to the experiment value of Noel *et al.*'s research on $CH_3NH_3SnI_3$.[8] The tin perovskite shows a p-type conducting behavior caused by the self-doping process of Sn^{2+}'s easy oxidization into Sn^{4+},[11] so we assume that the absorber is a p-type semiconductor doped with an initial carrier density of 3.2×10^{15} cm^{-3}.

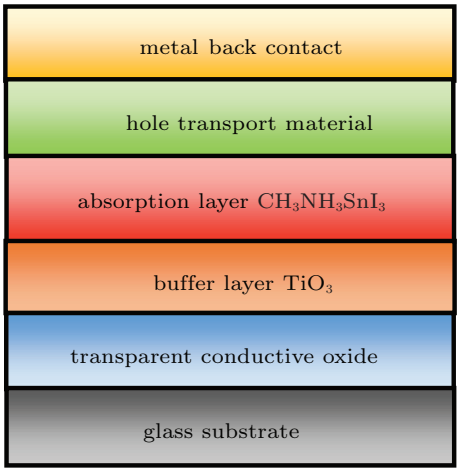


Fig. 1. (color online) Schematic diagram of the $CH_3NH_3SnI_3$PSC.

Table 1. Simulation parameters of $CH_3NH_3SnI_3$ PSC.

Parameters	TCO	TiO_2 (buffer)	$CH_3NH_3SnI_3$	spiro-OMeTAD (HTM)
Thickness/nm	500	30	350 (variable)	200
Band gap energy E_g/eV	3.5	3.2	1.3[9]	3.17[9]
Electron affinity χ/eV	4	4.26[9] (variable)	4.17[9]	2.05[9] (variable)
Relative permittivity ε_r	9	9	8.2[6]	3
Effective conduction Band Density N_c/cm^{-3}	2.20×10^{18}	2.00×10^{18}	1.00×10^{18}	2.20×10^{18}
Effective valence band density N_v/cm^{-3}	1.80×10^{19}	1.80×10^{19}	1.00×10^{18}	1.80×10^{19}
Electron mobility μ_n/(cm^2/V·s)	20	20	1.6[8]	2.00×10^{-4}
Hole mobility μ_p/(cm^2/V·s)	10	10	1.6[8]	2.00×10^{-4}
Donor concentration N_D/cm^{-3}	2.00×10^{19}	1.00×10^{16}		
Acceptor concentration N_A/cm^{-3}			3.20×10^{15} (variable)	2.00×10^{19}
Defect density N_t/cm^{-3}	1.00×10^{15}	1.00×10^{15}	4.50×10^{17} (variable)	1.00×10^{15}

Table 2. Parameters setting of interface defect and the defect in the absorber.[18,20]

Parameters and units	$CH_3NH_3SnI_3$	ETM/$CH_3NH_3SnI_3$ interface	$CH_3NH_3SnI_3$/HTM interface
Defect type	neutral	neutral	neutral
Capture cross section for	2.0×10^{-14}	1.0×10^{-15}	1.0×10^{-15}
Electrons and holes/cm^2	2.0×10^{-14}	1.0×10^{-15}	1.0×10^{-15}
Energetic distribution	Gaussian	single	single
Energy level with respect to E_v (above E_v , eV)	0.65	0.6	0.6
Characteristic energy/eV	0.1	~	~
Total density/cm^{-3}	1×10^{14}-10^{19}	1.0×10^{17}	1.0×10^{17}

With these initial parameters in Table 1, we study the current density–voltage (J-V) characteristic of the cell (see curve 1 in Fig. 2). The short-circuit current density (J_{sc}) of 18.67 mA/cm^2, open-circuit voltage (V_{oc}) of 0.68 V, fill factor (FF) of 47.43%, and power conversion efficiency (PCE) of 6.09% are obtained. The simulated device performance is consistent with the experimental values of the Tin-based PSCs,[9–11] certifying that the device simulation is valid and the input parameters that have been set are close to those for a real device. Due to the narrower band gap 1.3 eV of $CH_3NH_3SnI_3$ than 1.55 eV of $CH_3NH_3PbI_3$, the optical absorption edge of tin perovskite is red-shifted to 950 nm in the external quantum efficiency (QE) curve (see Fig. 3). The QE covers the entire visible spectrum and reaches a broad absorption maximum over 50% from 400 nm to 850 nm accompanied by a notable absorption onset up to 950 nm, which is in good accordance with the measured PCE spectrum of Ref. [22]. The red-shift of the QE curve is more beneficial to the light absorption at infrared wavelengths.

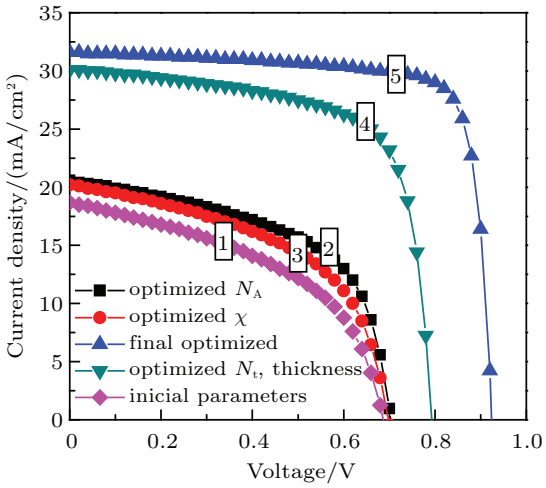


Fig. 2. (color online) J–V curve of the PSCs during the optimization.

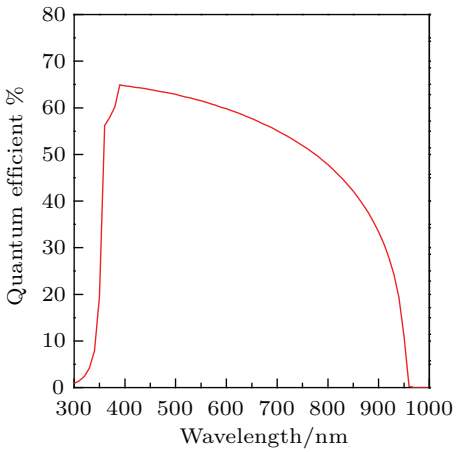


Fig. 3. (color online) External quantum efficiency curve of the PSC with the parameters in Table 1 and without considering the variation of the parameters.

In Section 3, based on the parameters above, the factors affecting the solar cell performance, such as the doping concentration, the defects density and the thickness for the perovskite absorber layer, the electron affinity χ of the ETM and the HTM, are studied in depth.

3. Results and discussion

3.1. Influence of doping concentration of perovskite absorption layer

$CH_3NH_3SnX_3$ (where X = Cl, Br, I) is unstable in ambient atmosphere: the Sn^{2+} ion will rapidly oxidize into more stable Sn^{4+} analogue,[9] which acts as a p-type dopant within the material in the "self-doping" process. Earlier studies on bulk $CH_3NH_3SnI_3$ show that the doping level can be varied greatly in a range of 10^{14} cm^{-3}–10^{19} cm^{-3} due to the presence of Sn^{4+} impurities.[9,10] In order to make it clear how the acceptor doping concentration (N_A) of the perovskite absorption layer can affect the performances of solar cells, $CH_3NH_3SnI_3$ layers with the values of N_A ranging from 10^{14} cm^{-3} to 10^{17} cm^{-3} are considered. Figure 4 provides the $PCEs$ of solar cells with different acceptor densities of the perovskite, and the maximum value of PCE appears at the N_A of 1.3×10^{16} cm^{-3}. The J_{sc} and V_{oc} are also related to the change of N_A for the perovskite, and both of them reach their maximum values when the N_A is approximately 1×10^{16} cm^{-3}. The external quantum efficiency (QE) significantly increases with the N_A of perovskite increasing from 10^{14} cm^{-3} to 10^{16} cm^{-3} (see Fig. 5), which implies that the generation rate of the photo-generated carriers increases under the same incident photon number. Hence, an appropriate doping concentration of the perovskite absorption layer is beneficial to the improvement of the photo-absorption efficiency and the J_{sc}. However, the V_{oc} drops rapidly when the N_A exceeds 1×10^{16} cm^{-3}. The variation in the cell performance with the doping concentration can be explained from the perspective of the built-in electric field which is enhanced with the increase of doping concentration. The enhancement of the electric field promotes the separation of carriers and then the improvement of the cell performance. However, further increasing the doping concentration will cause a higher Auger recombination rate, which is not beneficial to the increase of V_{oc}. It can be found from Fig. 6 that the recombination rate R increases significantly when the N_A exceeds 1×10^{16} cm^{-3}. Besides, the hole transportation will be greatly suppressed with the increase of p-type doping concentration of the perovskite absorption layer because of the enhanced impurity scattering and recombination. The quasi Fermi level of the hole (E_{Fp}) becomes far from the valence band top with the increase of N_A (see Fig. 7), even flattens into the E_{Fp} of the HTM. This affects the hole transportation strongly from the absorption layers to HTM, and the reduction of the hole density can also be seen from the E_{Fp} uplift of the perovskite absorption layer.

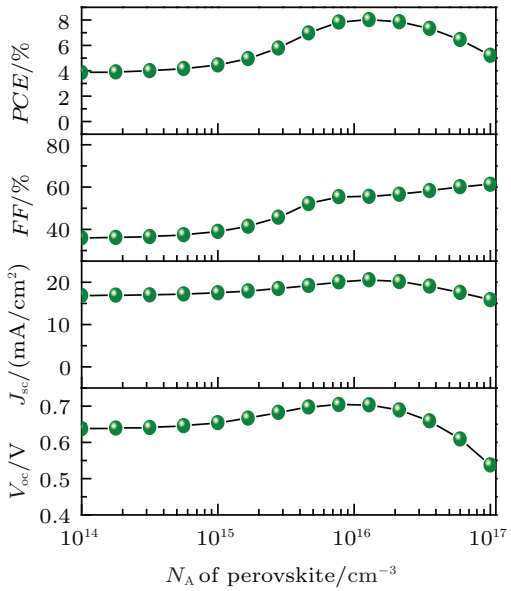


Fig. 4. (color online) Performance parameters of PSC with different acceptor densities of perovskite.

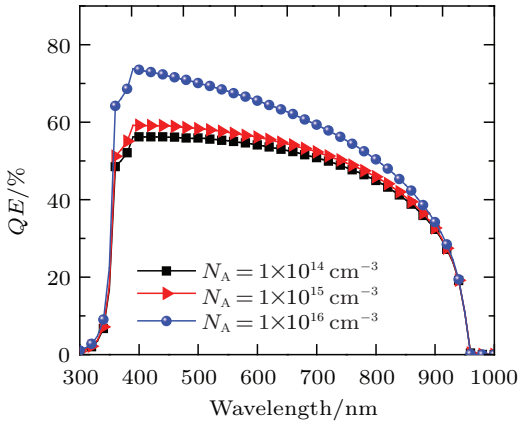


Fig. 5. (color online) Variations of external quantum efficiency (*QE*) with N_A of perovskite

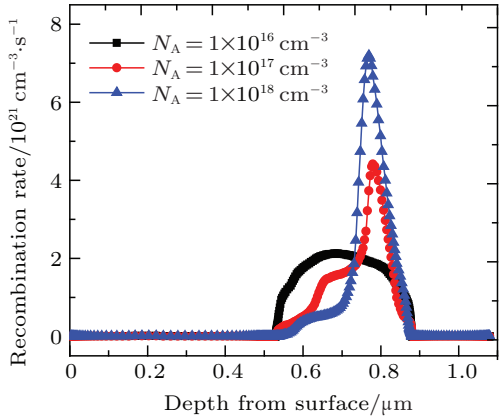


Fig. 6. (color online) Variation of recombination rate (*R*) with N_A of perovskite.

Consequently, only appropriate doping concentration can commendably improve the J_{sc} and V_{oc}, and then obtain a larger *PCE* value, and excessive doping concentration is unfavorable because of the increase of the recombination. The deposited films of tin perovskite must have low carrier concentration to maximize the carrier mobility within the active perovskite. Under the doping concentration of 1.3×10^{16} cm^{-3} for the perovskite absorption layer, the optimum cell performance with J_{sc} of 20.55 mA/cm^2, V_{oc} of 0.70 V, *FF* of 55.58%, and *PCE* of 8.03% is obtained (see Fig. 4).

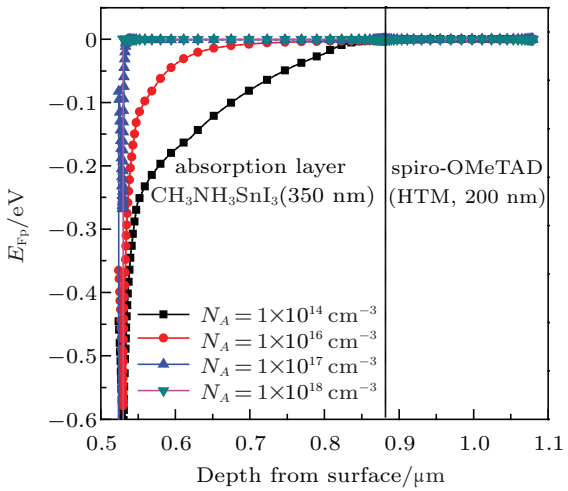


Fig. 7. (color online) Distributions of quasi Fermi level of the hole (E_{Fp}) for different values of N_A.

The comparison between current density–voltage curves with and without N_A optimization is shown in curves 2 and 1 of Fig. 2 respectively. At the optimum N_A of 1×10^{16} cm^{-3}, the *PCE* by 1.94% compared with that of the solar cell with an initial N_A of 3.2×10^{15} cm^{-3}. This consequence means that controlling the instability of Sn^{2+} oxidation state in perovskite layer and avoiding excessive Sn^{4+} in the perovskite are very important for optimizing the performance of the tin-based PSC. Experimental studies have shown that the addition of SnF_2 in the system reduces Sn^{4+} caused by the oxidation of Sn^{2+},[9] and the encapsulated device showed a stable performance with no significant drop in the absorbance for over 100 days.[9] This strategy is now commonly applicable to the fabrication of Sn-based PSC. These successful experiments indicate that with an appropriate fabrication and sealing process, the tin-based PSC with better stability can be obtained.

3.2. Influences of electron affinity of buffer and HTM

The band offset between buffer/absorption layers/HTM is a decisive factor of carrier recombination at the interface, which determines the open-circuit voltage (V_{oc}).[17] The band offsets are adjusted by varying the values of electron affinity (χ) of the buffer (3.8 eV–4.5 eV) and HTM (2.0 eV–2.9 eV). The variations of J_{sc}, V_{oc}, *FF*, and *PCE* with electron affinity value are shown in Figs. 8(a) and 8(b). A better solar cell *PCE* can be obtained at the χ values of 4.0 eV–4.2 eV for the buffer and 2.3 eV–2.6 eV for the HTM, respectively. A barrier cliff is formed at the absorber/HTM interface as shown in the inset of Fig. 9. The proper electron barrier cliff around 0.0 eV–0.2 eV does not affect the photo-generated electron flow toward a back electrode, and J_{sc} is almost constant. When the

$E_{\text{c-buffer}}$ is more than 0.2 eV higher than $E_{\text{c-absorber}}$, the collection of electrons is impeded by the raised barrier formed at the conduction band offset (see Fig. 9). This is because of the double-diode like curvature at higher conduction band offset.[17,23]

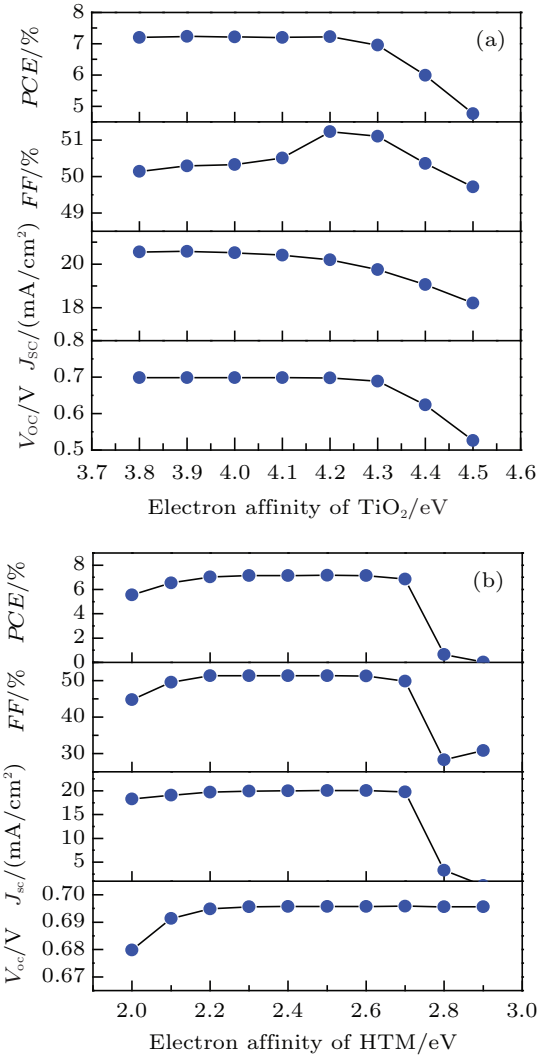


Fig. 8. (color online) Variations of performance parameters of PSC with electron affinity of buffer (a) and HTM (b).

Figure 8(b) shows the variations of the V_{oc} and the J_{sc} with the χ of HTM. The V_{oc} decreases when the $E_{v-\text{HTM}}$ is too low (lower than 2.2 eV), while the J_{sc} decreases when the $E_{v-\text{HTM}}$ is too high (higher than 2.7 eV). The optimum position of the $E_{v-\text{HTM}}$ is lower than that of the absorber by around 0.0 eV–0.3 eV and the χ of HTM is in a range of 2.3 eV–2.6 eV. The optimum properties of the solar cell of *PCE* of 7.21%, J_{sc} of 20.52 mA/cm^2, V_{oc} of 0.70 V, and *FF* of 50.33% are obtained when the electron affinity values of the buffer and HTM are set to be 4.0 eV and 2.6 eV respectively. Obvious improvement of the voltage-current characteristics can be seen from the *J*–*V* curves with the band offset optimization (see curve 3 in Fig. 2). The simulation results of the electron affinity of buffer and HTM are similar to those from the band offset study on $CH_3NH_3PbI_3$PSCs in Ref. [17], and they also found that selecting buffers and HTMs with suitable electron affinity can inhibit the interface recombination and help to further optimize the solar cells performance.

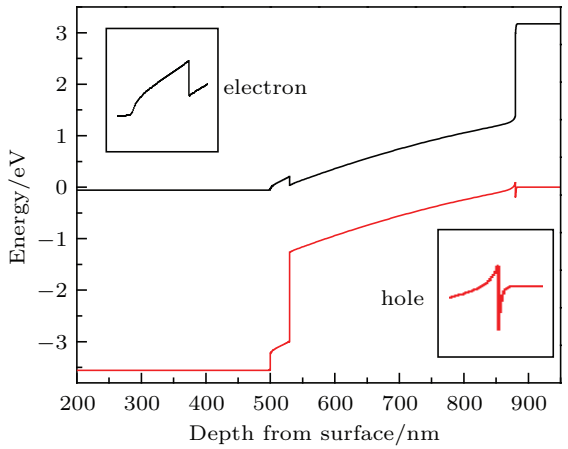


Fig. 9. (color online) Energy band diagrams of perovskite solar cells with charge barriers at the buffer/absorber /HTM interfaces. Insets show close-up images at the interface.

3.3. Influence of defect density and thickness of perovskite absorption layer

The efficiency of the solar cell can be improved to a certain extent by adjusting the electron affinity values of buffer and HTM or the p-type carrier concentration of perovskite. In order to further improve the PSC performance, another affecting parameter, the defect density of the perovskite layer, should be considered. The morphology and quality of the perovskite film have been recognized recently as an important factor determining perovskite solar cell performance,[24,25] since the photoelectrons are mainly generated in this light-absorber layer. Poor film quality and coverage of the tin perovskite on the mesoporous TiO_2 electrodes have been observed.[10] The charge recombination behaviors will become dominant in the light-absorber layer because of the larger defect density (N_{t}) caused by the poor film quality, which can determine the V_{oc} of the device. The study about the influence of the defect density of the perovskite layer on cell performance is based on the Shockley–Read–Hall recombination model (SRH). The neutral defects with Gaussian distribution and characteristic energy of 0.1 eV are set to be at the center of the band gap. The SRH recombination model is as follows:[26,27]

$$R = \frac{np - n_i^2}{\tau_{\text{p}}(n + N_{\text{C}}\,\text{e}^{(E_{\text{g}}-E_{\text{t}})/kT} + \tau_n(p + N_{\text{V}}\,\text{e}^{E_{\text{t}}/kT})}, \qquad (1)$$

where n and p are the concentrations of the mobile electrons and the holes, which can be obtained from solving the Poisson equation and the continuity equation for the charge carriers. For sufficient forward bias, i.e., $qV > 3kT$, we can neglect the term n_i^2, which is from the thermal generation. E_{t} and N_{t} are the energy level and concentration of the trap defects respectively. $\tau_{\text{n,p}}$ is the lifetime for the electrons and holes, and can

be given by

$$\tau_{n,p} = \frac{1}{\sigma_{n,p} \upsilon_{th} N_t}, \tag{2}$$

where $\tau_{n,p}$ and $\sigma_{n,p}$ are the lifetime and the capture cross-section of the electrons and holes respectively and v_{th} is the thermal velocity. The carrier diffusion length l can be given by

$$l = \sqrt{D\tau}, \tag{3}$$

where D is the diffusion coefficient and can be given by

$$D = \mu kT/q, \tag{4}$$

where μ is the carrier mobility. With formula (2)–(4), combining with the relative parameters of the carriers, we can obtain the diffusion lengths of the electrons (l_n) and holes (l_p). The simulated values of l_n and l_p are the same, because all the parameters for the electron and hole in the absorber, such as the thermal velocity, the capture cross section, and the mobility (1.6 $cm^2/V{\cdot}s$, from literature[9]) are set to be the same as those in Table 2,[17] which is consistent with ambipolar characteristics of the carriers.[24] In the actual situation the diffusion length l_p of the holes is slightly shorter than l_n of the electrons because of the larger effective mass of the hole. Nonetheless, these values of l_n and l_p for perovskite are relatively balanced compared with typical values reported in bulk heterojunction solar cells, where the electron and hole transport lengths (proportional to their mobility) differ by orders of magnitude.[25] These balanced long charge-carrier diffusion lengths would account for the remarkable performances reported for these perovskite devices. Ignoring the difference between l_n and l_p, and only focusing on the effect of the defect on the carrier transportation, have little influence on the validity of the simulation.

The initial defect density N_t of the absorber is set to be 4.5×10^{17} cm^{-3}, because on this condition the simulated carrier diffusion length of 30 nm is similar to the experiment value of Noel *et al.*'s research on $CH_3NH_3SnI_3$.[8] Based on previous simulated studies of lead perovskite,[17,19,21] we change defect density N_t from 10^{14} cm^{-3} to 10^{19} cm^{-3} and depict the variation of photovoltaic property with N_t in Fig. 10. The performance of the device is improved significantly with the reduction of the defect density in perovskite, which is consistent with the numerical simulation of the lead perovskite.[21] When defect density is as low as 1×10^{15} cm^{-3} the cell performance is significantly improved attaining the J_{sc} of 28.48 mA/cm^2, V_{oc} of 0.79 V, *FF* of 67.60% and *PCE* of 15.28%. Further decrease of the N_t from 10^{15} cm^{-3} to 10^{14} cm^{-3}, the improvement of the cell performance is slight. The realization of such low N_t of 10^{14} cm^{-3} in experiment is very difficult so we set the defect density of 1×10^{15} cm^{-3} as an optimized value, and all the values of J_{sc}, V_{oc}, *FF* and *PCE* approximately reach their maxima with this defect density. Experimental studies have shown that the tin-based perovskite displays good charge-transport properties.[28,29] In order to understand the influence of the defect density N_t on the cell performance deeply, we study the effects of defect density on the carrier diffusion length l and the recombination rate R (see Table 3 and Fig. 11) based on the SRH recombination model and the formula of l. When the N_t is lower, the diffusion length l is longer and the recombination rate R is lower, which is conducible to the improvement of the cell performance.

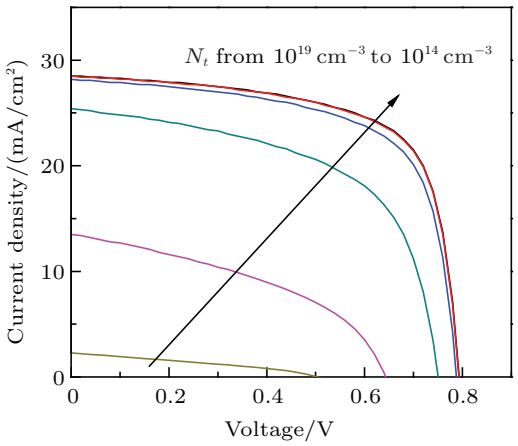


Fig. 10. (color online) Current density-voltage curves, with increasing the value of N_t.

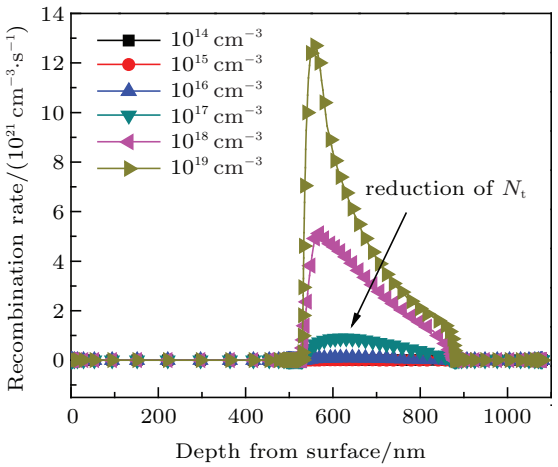


Fig. 11. (color online) Variations of the recombination rate with depth from surface for different values of N_t.

Table 3. Variations of the diffusion length with defect density.

N_t/cm^{-3}	1×10^{14}	4×10^{14}	1.6×10^{15}	4×10^{16}	1.6×10^{17}
$l_n(l_p)/\mu m$	2	1	0.5	0.1	0.05

The thickness of the light-absorbing layer plays a crucial role in determining the performance of thin-film solar cells.[30] The variation of the cell performance with the thickness of the absorption layer is shown in Fig. 13. When the thickness is too low, it is not beneficial to the full absorption of the light and causes the lower cell *PCE*. With the increase of the thickness of the absorber, the *PCE* improves gradually. When the thickness is larger than 600 nm, the *PCE* of the cell remains invariable. If the absorber layer is too thick, the photogenerated carriers cannot be collected effectively because they must

travel through the absorber to reach the carrier collecting layers before they are recombined. The charge diffusion length is critical in designing the perovskite layer thickness and structure. The influences of the thickness of the perovskite absorption layer with different charge diffusion lengths on the solar cell performance are shown in Fig. 14.

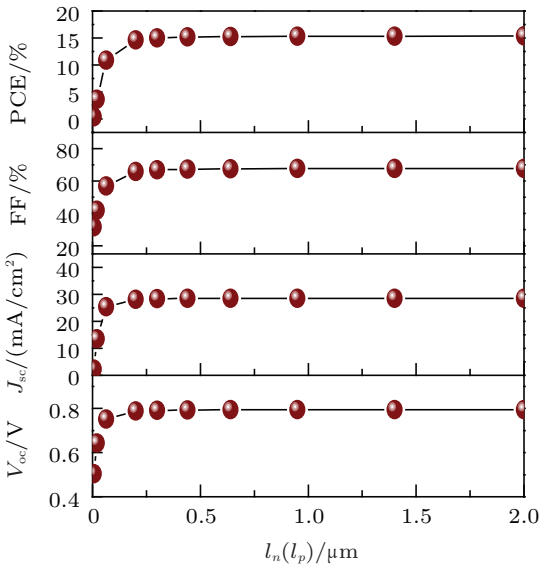


Fig. 12. (color online) Variations of cell performance, with increasing the diffusion length l.

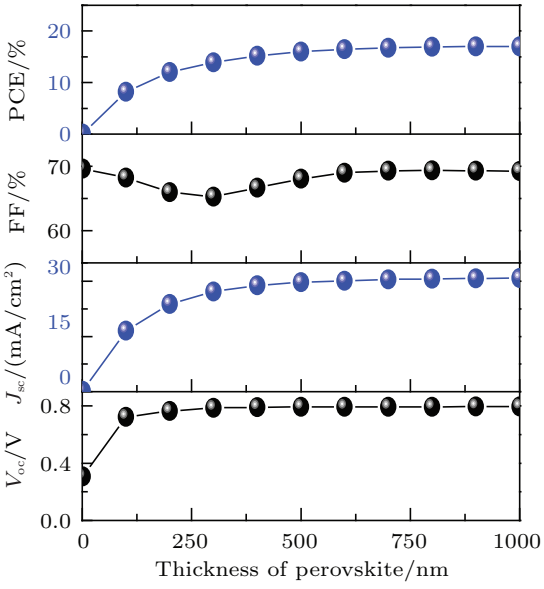


Fig. 13. (color online) Variations of the cell performance with perovskite thickness.

The *PCE* of the cell gradually increases with the increase of the thickness of the absorber, but when the thickness is larger than 600 nm, the growth of the *PCE* slows down. Taking into consideration the influence of the N_t and the thickness of the absorber, the performance parameters of devices are optimal when N_t is as low as 1×10^{15} cm^{-3} (l of 0.6 μm) and the thickness is 600 nm for the perovskite layer, and reach the J_{sc} of 30.14 mA/cm^2, V_{oc} of 0.79 V, *FF* of 68.96% and *PCE* of 16.50% (see line 4 in Fig. 2), resulting in better cell performance than the initial cell performance. This significant performance improvement of the cell with the N_t reduction is attributed to the lower recombination of the carriers and the longer l (see Figs. 11 and 12).

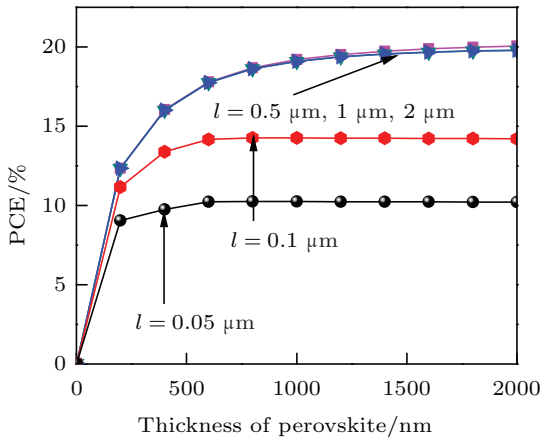


Fig. 14. (color online) Variations of *PCE* with perovskite thickness for different values of diffusion length l of the carriers.

The simulation shows that N_t is an important factor determining the performance of perovskite solar cells, and this result consists with the research about $CH_3NH_3PbI_3$ perovskite cell.[21] Experimental researchers have obtained the uniform, pinhole-free $CH_3NH_3SnI_3$ perovskite films from a strongly coordinating solvent such as dimethyl sulfoxide (DMSO).[11] Introduction of pyrazine also can provide beneficial effects for improving the surface morphology and preventing the unwanted Sn oxidation.[31] Besides, by a new variant of pulsed excimer laser deposition: a room-temperature dry process, the growth of good quality lead-free $CH_3NH_3SnI_3$ films is also demonstrated.[31] Finally, we consider all of the factors (N_A, χ, N_t, thickness) discussed above in Subsections 3.1–3.3 (see Table 4) depict current density-voltage curves (see curve 5 in Fig. 2), and obtain encouraging results of the J_{sc} of 31.59 mA/cm^2, V_{oc} of 0.92 V, *FF* of 79.99% and *PCE* of 23.36%. Our simulation shows that the lead-free $CH_3NH_3SnI_3$ perovskite solar cells with high efficiency can be achieved by adjusting the doping concentration and the defect density of the absorption layer, and the electron affinity of each of ETM and HTM. Especially the reduction of the defect density in the perovskite layer can improve the cell performance significantly.

Table 4. Final optimized parameters of $CH_3NH_3SnI_3$ PSC.

Optimized parameters	buffer	$CH_3NH_3SnI_3$	HTM
χ/eV	4.0	–	2.6
N_A/cm^{-3}	–	1.3×10^{16}	–
N_t/cm^{-3}	–	1.0×10^{15}	–
Thickness/nm		600	

It should be noted that the *PCE* of the lead-free perovskite solar cell is still lower than that of the reported high-efficiency $CH_3NH_3PbI_3$ perovskite solar cells in the present experimental studies, and this might be related to the poor quality of

perovskite film and the low coverage on the mesoporous TiO_2 electrode. The simulation in this paper shows that further efficiency enhancement of the lead-free PSCs would be expected by reducing the defect density and improving the stability of $CH_3NH_3SnI_3$ in the future.

4. Conclusions

The lead-free $CH_3NH_3SnI_3$ perovskite solar cells with different parameters are analyzed by using one-dimensional device simulation in this work. The results indicated that the appropriate p-type carrier doping concentration of tin perovskite could improve the *PCE* of the device because of the enhanced built-in electric field, but excessive concentration can lead to a higher recombination rate and poor cell performance; adjusting the electron affinity of buffer and HTM to provide an appropriate interface barrier of carriers can reduce the interface recombination and improve the *PCE* of the device to some extent. The defect density of the perovskite is the most critical factor in the simulation for high efficiency of solar cells, and reducing the density concentration as low as 1×10^{15} cm^{-3} can significantly increase the *PCE* of the device from 6.09% to 15.28%. The optimized perovskite thickness of 600 nm can absorb more light and increase the *PCE* of the device to 16.50%. Encouraging results with *PCE* of 23.36% are obtained by optimizing all of the factors mentioned above. The results show that the lead-free $CH_3NH_3SnI_3$ perovskite solar cells have the potential to be highly efficient PSCs. By reducing the defect density and improving the stability of Sn^{2+} in $CH_3NH_3SnI_3$through optimizing the fabrication and encapsulation process, further efficiency enhancements of the lead-free $CH_3NH_3SnI_3$ perovskite solar cells would be expected.

References

[1] Kazim S, Nazeeruddin M K, Gratzel M and Ahmad S 2014 *Angew. Chem. Int. Ed.* **53** 2812

[2] Lotsch B V 2014 *Angew. Chem. Int. Ed.* **53** 635

[3] Wei Z H, Chen H N, Yan K Y and Yang S H 2014 *Angew. Chem. Int. Ed.* **53** 13239

[4] Kojima A, Teshima K, Shirai Y and Miyasaka T 2009 *J. Am. Chem. Soc.* **131** 6050

[5] NRELchart2016http:www.nrel.govncpvimagesefficiency chart.jpg [6] Stoumpos C C, Malliakas C D and Kanatzidis M G 2013 *Inorg. Chem.* **52** 9019

[6] Umari P, Mosconi E and De Angelis F 2014 *Sci. Rep.* **4** 4467

[7] Chen Q Y, Huang Y, Huang P R, Ma T, Cao C and He Y 2016 *Chin. Phys. B* **25** 027104

[8] Noel N K, Stranks S D, Abate A, Wehrenfennig C, Guarnera S, Haghighirad A A, Sadhanala A, Eperon G E, Johnston M B, Petrozza A M, Herz L M and Snaitha H J 2014 *Energy Environ. Sci.* **9** 3061

[9] Hao F, Stoumpos C C, Cao D H, Chang R P H and Kanatzidis M G 2014 *Nat. Photon.* **8** 489

[10] Hao F, Stoumpos C C, Guo P, Zhou N, Marks T J, Chang R P H and Kanatzidis M G 2015 *J. Am. Chem. Soc.* **137** 11445

[11] Koh T M, Krishnamoorthy T, Yantara N, Shi C, Leong W L, Boix P P, Grimsdale A C, Mhaisalkar S G and Mathews N 2015 *J. Mater. Chem. A.* **3** 14996

[12] Marshall K P, Walton R I and Hatton R A 2015 *J. Mater. Chem. A* **3** 11631

[13] Kumar M H, Dharani S, Leong W L, Boix P P, Prabhakar R R, Baikie T, Shi C, Ding H, Ramesh R, Asta M, Graetzel M, Mhaisalkar S G and Mathews N 2014 *Adv. Mater.* **26** 7122

[14] Lang L, Yang J H, Liu H R, Xiang H J and Gong X G 2014 *Phys. Lett. A* **378** 290

[15] Zhu J Z Qi L H Du H J and Chai Y C 2015 *Chin. Phys. B* **24** 108501

[16] Minemoto T and Murata M 2015 *Sol. Energy Mat. Sol. Cells.* **133** 8

[17] Kemp K W, Labelle A J, Thon S M, Ip A H, Kramer I J, Hoogland S and Sargent E H 2013 *Adv. Energy Mater.* **3** 917

[18] Minemoto T, and Murata M 2014 *J. Appl. Phys.* **116** 054505

[19] Minemoto T, and Murata M 2014 *Curr. Appl. Phys.* **14** 1428

[20] Liu F, Zhu J, Wei J, Li Y, Lv M, Yang S, Zhang B, Yao J and Dai S 2014 *Appl. Phys. Lett.* **104** 253508

[21] Hao F Stoumpos C C Chang R P H and Kanatzidis M G 2014 *J. Am. Chem. Soc.* **136** 8094

[22] Scheer R 2009 *J. Appl. Phys.* **105** 104505

[23] Ball J M Lee M M, Hey A and Snaith H J 2013 *Energ. Environ. Sci.* **6** 1739

[24] Xing G C, Mathews N, Sun S Y, Lim S S, Lam Y M, Grätzel M, Mhaisalkar S and Sum T C 2013 *Science* **342** 344

[25] Hall R N 1953 *Proc. Phys. Soc.* **24** 221

[26] Shockley W and Read W T 1952 *Phys. Rev.* **87** 835

[27] Kagan C R, Mitzi D B and Dimitrakopoulos C D 1999 *Science* **286** 945

[28] Mitzi D B, Wang S, Feild C A, Chess C A and Guloy A M 1995 *Science* **267** 1473

[29] Liu D Y, Gangishetty M K and Kelly T L 2014 *J. Mater. Chem. A* **2** 19873

[30] Lee S J, Shin S S, Kim Y C, Kim D, Ahn T K, Noh J H, Seo J and Seok S I 2016 *J. Am. Chem. Soc.* **138** 3974

[31] Bansode U, Naphade R, Game O, Agarkar S and Ogale S 2015 *J. Phys. Chem. C* **119** 9177